Denia, FD.; Martínez Casas, J.; Carballeira, J.; Nadal, E.; Fuenmayor Fernández, FJ. (2018). Computational performance of analytical methods for the acoustic modelling of automotive exhaust devices incorporating monoliths. Journal of Computational and Applied Mathematics. 330:995-1006. https://doi.org/10.1016/j.cam.2017.03.010

Computational performance of analytical methods for the acoustic modelling of automotive exhaust devices incorporating monoliths

F. D. Denia, J. Martínez-Casas, J. Carballeira, E. Nadal, F. J. Fuenmayor*
Centro de Investigación en Ingeniería Mecánica, Universitat Politècnica de València, Camino de Vera s/n, 46022 Valencia, Spain

***Corresponding author:**
Dr. F. D. Denia
Centro de Investigación en Ingeniería Mecánica
Universitat Politècnica de València
Camino de Vera s/n
46022 Valencia
Spain
Tel: +34 96 387 70 07 Ext: 76225
Fax: +34 96 387 76 29
e-mail: fdenia@mcm.upv.es

ABSTRACT

The acoustic modelling of automotive exhaust devices, such as catalytic converters (CC) and diesel particulate filters (DPF), usually requires the use of multidimensional analytical and numerical techniques. The presence of higher order modes and three-dimensional waves in the expansion and contraction subdomains, as well as sound propagation within the monolith capillary ducts, can be considered through the finite element method (FEM), although this approach is traditionally thought to be very time consuming. With a view to overcome this limitation and to reduce the computational effort of the FEM, alternative modelling techniques are presented in the current work to speed up transmission loss calculations in exhaust devices incorporating monoliths. These approaches are based on the point collocation technique and the mode matching method. As shown in earlier studies, the sound attenuation of an exhaust device incorporating a monolith can be properly predicted if the latter is replaced by a plane wave four-pole transfer matrix providing a relationship between the acoustic fields at both sides of the monolithic region. Therefore, this work combines the presence of multidimensional higher order modes in the expansion and contraction regions with one-dimensional wave propagation within the capillary ducts of the central monolith. The point collocation technique and the mode matching method are applied to the compatibility conditions of the acoustic fields at all the subdomain interfaces to couple the solutions of the wave equation in the corresponding exhaust device subcomponents. For the particular case of rigid circular ducts, Bessel functions are considered as transversal pressure modes. The computational efficiency and accuracy of the results associated with the two analytical modelling techniques presented here are assessed, including the effect of the number of modes and collocation points, as well as their location. All the analytical approaches proposed in this work provide accurate predictions of the device attenuation performance and outperform the computational expenditure of a FE computation. Some differences are found, however, among the various analytical schemes in terms of computational speed and solution accuracy. From the results presented here, the mode matching method is the most efficient technique for the particular configurations under study, mainly due to the possibility of exploiting the orthogonality properties of the transverse pressure modes.

Keywords: Acoustic Modelling; Sound Attenuation; Transmission Loss; Automotive Exhaust Device; Monolith; Catalytic Converter; Mode Matching Method; Point Collocation Technique; Transfer Matrix; Finite Element Method; Computational Performance.

1. INTRODUCTION

As a result of increasing limitations on pollutant emissions, the use of after-treatment devices such as catalytic converters and diesel particulate filters has become a necessary practice in the design of the vehicle exhaust system. Although the design of these devices focuses mainly on the control of emissions (CO, NOx, HC and soot particles) [1], the acoustic aspects associated with catalysts and particulate filters also play a relevant role and have to be taken into account in the integral design of automotive exhaust systems from the point of view of noise control [2-4]. Therefore, not only noise attenuation due to silencers, but also the influence of catalytic converters and filters, should be considered in the development of analytical and numerical tools for predicting the acoustic behaviour of the complete exhaust system. For this reason, a number of publications can be found associated with the acoustic modelling of these devices [2-9].

One of the most relevant characteristics in both catalysts and particulate filters is the use of a ceramic monolith [1], formed by thousands of capillary tubes with very small cross dimensions. On one hand, the sound propagation phenomena inside the monolith must be evaluated, where the viscothermal interaction between the air and the capillary tube walls is of special relevance. Kirchhoff [10] presented a detailed propagation model for stationary medium. Zwikker and Kosten [11] later obtained relevant solutions for this model in the case of capillaries with circular cross-section. Of more practical interest are the rectangular sections, taken into account in the works of Stinson [12] and Roh et al. [13]. The presence of mean flow was considered by Dokumaci [14], who extended the work of Zwikker and Kosten [11] and obtained a simple analytical solution for propagation in circular capillaries including moving medium. In a later work, the same author presented an analytical solution for rectangular capillaries of small transverse dimensions, again in the presence of mean flow [15].

On the other hand, both the development and the implementation of sound wave propagation prediction tools inside complete exhaust devices such as CC and DPF additionally require acoustic models for the expansion chambers and inlet/outlet ducts, located at both sides of the monolith. The traditional plane wave models [14-16] have important limitations and are only applicable in the low frequency range and for relatively small cross-sectional ducts [16]. For these reasons, and in order to have higher accuracy in the analysis, a number of multidimensional numerical models [7, 8, 17] and analytical approaches [5, 6, 9] have been developed in the last decades, the latter providing a lower computational effort. Multidimensional schemes can be subdivided into two large groups.

First, the so-called 3D cavities/3D monolith, usually less realistic, in which multidimensional propagation is considered in the expansion chambers and inlet/outlet ducts as well as in the capillaries of the monolith [17]. To do so, it is assumed that the monolith resembles, acoustically speaking, a sound absorbent material with homogeneous and isotropic behaviour, defined by complex and frequency-dependent equivalent properties, such as the density and speed of sound [18]. Secondly, the more realistic 3D cavities/1D monolith technique, which retains multidimensional propagation in the expansion chambers and inlet/outlet ducts, but assumes one-dimensional acoustic behaviour within the capillaries and thus ignores any possible three-dimensionality of the sound field within the monolith [4-9,17]. From a mathematical point of view, this second approach therefore allows the replacement of the ceramic monolith by a plane wave four-pole transfer matrix and only the presence of plane waves in the monolith occurs, which seems more consistent with the one-dimensional characteristics of the capillary tubes integrating the CC.

In this work, the 3D cavities/1D monolith technique is combined with the point collocation technique [9, 16, 19-24] and the mode matching method with weighted integration [5, 6, 25-30] to reduce the computational cost of FEM-based numerical tools [2, 8, 16, 31-33]. The analytical approaches developed in previous publications, mainly related to silencers, are extended here to combine the propagation of multidimensional higher order modes in the chambers and ducts (forming the inlet expansion and the outlet contraction), with the one-dimensional model for the capillary tubes of the central monolith. The coupling of the solutions of the wave equation in the different subdomains is carried out based on the compatibility conditions of the pressure and axial velocity fields at the interfaces of the geometrical discontinuities. These compatibility conditions are enforced point-wise (point collocation) as well as in the form of a weighted integral (mode matching). The analytical results obtained through both techniques are validated, for a particular cylindrical configuration, by comparison with numerical simulations based on the FEM, exhibiting a good agreement and a lower computational expenditure. In addition, both analytical approaches are compared, which shows the advantages of the mode matching method over the point collocation technique in terms of computation time and accuracy, mainly due to the possibility of exploiting the orthogonality properties of the transversal pressure modes [16, 25-29, 34]. Finally, the influence of the location of the collocation points on the computational numerical performance is also studied.

2. MATHEMATICAL APPROACH

2.1. Acoustic model

Fig. 1 shows a scheme of an automotive exhaust device incorporating a monolith. The geometry is divided into several subdomains: regions *A* and *B* are associated with the inlet duct and the expansion chamber, respectively, while regions *D* and *E* form the contraction. These ducts and chambers have an axially uniform cross-section, and the corresponding propagation medium (air) is characterized by its density and speed of sound, denoted by ρ_0 and c_0, respectively. As indicated previously, the acoustic fields can be multidimensional in regions *A*, *B*, *D* and *E*. On the other hand, a monolith is placed in the central part of the device, consisting of capillaries with small cross-section. The acoustic propagation in these capillary ducts is basically one-dimensional and can be characterized by a four-pole matrix (see Fig. 1) in terms of complex and frequency-dependent equivalent properties ρ_m and c_m [18, 34].

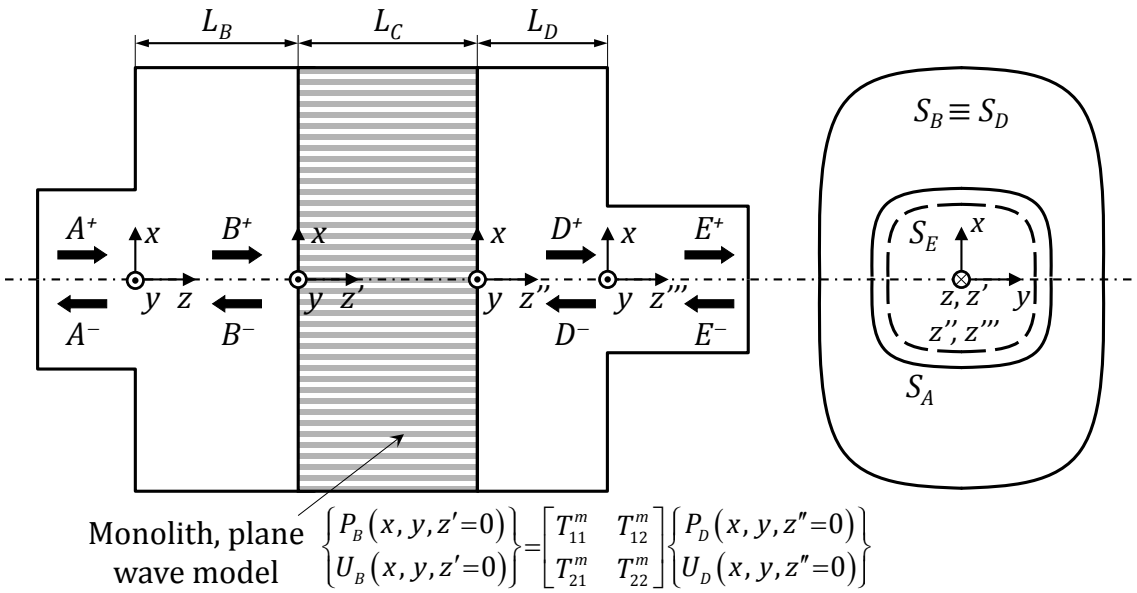

Fig. 1. Scheme of an automotive exhaust device incorporating a monolith. The latter is replaced by a transfer matrix to model its acoustic behaviour.

To completely define the acoustic field inside the device, it is necessary to solve the wave equation [16, 34, 35]. For the rigid wall duct *A* (and also *B*, *D* and *E* with the appropriate modifications), the solution can be written in terms of a modal expansion as [16, 22, 24-29]

$$P_A(x,y,z) = \sum_{n=1}^{\infty} \left(A_n^+ \, \mathrm{e}^{-\mathrm{j}k_{A,n}z} + A_n^- \, \mathrm{e}^{\mathrm{j}k_{A,n}z} \right) \psi_{A,n}(x,y), \tag{1}$$

$$U_A(x,y,z)=\frac{1}{\rho_0\,\omega}\sum_{n=1}^{\infty}k_{A,n}\left(A_n^{+}\,\mathrm{e}^{-\mathrm{j}k_{A,n}z}-A_n^{-}\,\mathrm{e}^{\mathrm{j}k_{A,n}z}\right)\psi_{A,n}(x,y), \tag{2}$$

where P_A and U_A are the acoustic pressure and axial velocity fields, A_n^{+} and A_n^{-} are the modal amplitudes (unknowns of the problem) associated with incident and reflected waves, $\psi_{A,n}(x,y)$ is the transversal pressure mode corresponding to cross-section under analysis, $k_{A,n}$ is the axial wavenumber, ω is the angular frequency, ρ_0 is the density of the air, and j is the imaginary unit.

The computation of the unknown modal amplitudes $A_n^{\pm}$, $B_n^{\pm}$, $D_n^{\pm}$ and $E_n^{\pm}$ in all the regions to obtain a complete description of sound propagation inside the exhaust device requires the acoustic fields to be matched at the geometrical discontinuities. These include the sudden expansion between the inlet duct *A* and the chamber *B*, the interfaces of chambers *B* and *D* at both sides of the monolith, and the sudden contraction between the chamber *D* and the outlet pipe *E*. Compatibility conditions are provided by the following physical requirements: continuity of acoustic pressure and axial velocity at the expansion/contraction, zero axial velocity normal to the rigid endplates, and coupling of acoustic pressures and axial velocities at both sides of the monolith by a plane wave four-pole transfer matrix [2, 6-8, 34].

Therefore, at the expansion of the geometry the continuity of acoustic pressure and axial velocity are expressed as

$$P_A(x,y,z=0)=P_B(x,y,z'=-L_B)\qquad (x,y)\in S_A, \tag{3}$$

$$U_A(x,y,z=0)=U_B(x,y,z'=-L_B)\qquad (x,y)\in S_A, \tag{4}$$

while the zero axial velocity at left end rigid plate is given by

$$U_B(x,y,z'=-L_B)=0\quad (x,y)\in S_B-S_A. \tag{5}$$

The acoustic coupling associated with the monolith at the interfaces $S_B\equiv S_D$ yields

$$P_B(x,y,z'=0)=T_{11}^{m}P_D(x,y,z''=0)+T_{12}^{m}U_D(x,y,z''=0)\qquad (x,y)\in S_B\equiv S_D, \tag{6}$$

$$U_B(x,y,z'=0)=T_{21}^{m}P_D(x,y,z''=0)+T_{22}^{m}U_D(x,y,z''=0)\qquad (x,y)\in S_B\equiv S_D, \tag{7}$$

or, in matrix form

$$\begin{Bmatrix} P_B(x,y,z'=0) \\ U_B(x,y,z'=0) \end{Bmatrix} = \begin{bmatrix} T_{11}^m & T_{12}^m \\ T_{21}^m & T_{22}^m \end{bmatrix} \begin{Bmatrix} P_D(x,y,z''=0) \\ U_D(x,y,z''=0) \end{Bmatrix} \qquad (x,y) \in S_B \equiv S_D, \tag{8}$$

where T_{11}^m, T_{12}^m, T_{21}^m and T_{22}^m are the so-called monolith acoustic four-poles [16, 34].

Finally, the contraction yields similar equations to those written for the expansion. The continuity of acoustic pressure and axial velocity gives

$$P_D(x,y,z''=L_D) = P_E(x,y,z'''=0) \qquad (x,y) \in S_E, \tag{9}$$

$$U_D(x,y,z''=L_D) = U_E(x,y,z'''=0) \qquad (x,y) \in S_E, \tag{10}$$

and the zero axial velocity at right end rigid plate leads to

$$U_D(x,y,z''=L_D) = 0 \qquad (x,y) \in S_D - S_E. \tag{11}$$

In the following sections, the equations obtained by the application of the point collocation technique and the mode matching method will be presented. Special attention will be paid to the particular case of ducts with circular cross-section. For this geometry, the transversal modes of pressure are given by Bessel functions [16, 25-28, 34] and an analytical treatment is possible, leading to a considerable reduction of the computational effort (for example, when integrating products of modes in the mode matching method [6, 25-28]). Other geometries of practical interest, such as rectangular and elliptical ducts, will also allow an analytical description of the transversal modes [16, 36]. For geometries with arbitrary cross-section, a two-dimensional FEM can be used to calculate such modes [22, 24] and numerical schemes can be considered for computing the mode matching integrals [27, 29].

2.2. Point collocation technique

Eqs. (3)-(11) are enforced at discrete points in this section. A number of modes N_m is considered to expand the acoustic pressure and velocity fields, Eqs. (1) and (2), for regions *B* and *D*, associated with the chambers, while N_a and N_e are taken into account for the inlet and outlet ducts *A* and *E*, respectively.

2.2.1. Expansion

The continuity of pressure, Eq. (3), is enforced at N_a points over S_A given by coordinates (x_p, y_p, $z = 0$) in duct *A* and coordinates (x_p, y_p, $z' = -L_B$) in chamber *B*, with $p = 1, 2, \ldots, N_a$. This yields the following set of equations

$$\sum_{n=1}^{N_a}\left(A_n^+ + A_n^-\right)\psi_{A,n}\left(x_p, y_p\right) = \sum_{n=1}^{N_m}\left(B_n^+ \mathrm{e}^{-\mathrm{j}k_{B,n}(-L_B)} + B_n^- \mathrm{e}^{\mathrm{j}k_{B,n}(-L_B)}\right)\psi_{B,n}\left(x_p, y_p\right). \quad (12)$$

The continuity of axial acoustic velocity defined by Eq. (4) is considered at the same N_a points with coordinates (x_p, y_p, $z = 0$) and (x_p, y_p, $z' = -L_B$) over S_A, giving for $p = 1, 2, \ldots, N_a$

$$\sum_{n=1}^{N_a} k_{A,n}\left(A_n^+ - A_n^-\right)\psi_{A,n}\left(x_p, y_p\right) = \sum_{n=1}^{N_m} k_{B,n}\left(B_n^+ \mathrm{e}^{-\mathrm{j}k_{B,n}(-L_B)} - B_n^- \mathrm{e}^{\mathrm{j}k_{B,n}(-L_B)}\right)\psi_{B,n}\left(x_p, y_p\right). \quad (13)$$

For the left end rigid plate characterized by Eq. (5), $N_m - N_a$ points are chosen over $S_B - S_A$. The corresponding coordinates are (x_p, y_p, $z' = -L_B$), with $p = 1, 2, \ldots, N_m - N_a$, leading to

$$\sum_{n=1}^{N_m} k_{B,n}\left(B_n^+ \mathrm{e}^{-\mathrm{j}k_{B,n}(-L_B)} - B_n^- \mathrm{e}^{\mathrm{j}k_{B,n}(-L_B)}\right)\psi_{B,n}\left(x_p, y_p\right) = 0. \quad (14)$$

2.2.2. Monolith

The four-pole relation given by Eqs. (6)-(8) is prescribed at N_m points over $S_B \equiv S_D$, establishing a point-wise connection between both sides of the monolith. The particular coupling expressions between the acoustic fields at coordinates (x_p, y_p, $z' = 0$) and (x_p, y_p, $z'' = 0$), with $p = 1, 2, \ldots, N_m$, for regions B and D respectively, are given by

$$\begin{aligned}&\sum_{n=1}^{N_m}\left(B_n^+ + B_n^-\right)\psi_{B,n}\left(x_p, y_p\right)\\ &= T_{11}^m \sum_{n=1}^{N_m}\left(D_n^+ + D_n^-\right)\psi_{D,n}\left(x_p, y_p\right) + \frac{T_{12}^m}{\rho_0 \omega}\sum_{n=1}^{N_m} k_{D,n}\left(D_n^+ - D_n^-\right)\psi_{D,n}\left(x_p, y_p\right),\end{aligned} \quad (15)$$

$$\begin{aligned}&\frac{1}{\rho_0 \omega}\sum_{n=1}^{N_m} k_{B,n}\left(B_n^+ - B_n^-\right)\psi_{B,n}\left(x_p, y_p\right)\\ &= T_{21}^m \sum_{n=1}^{N_m}\left(D_n^+ + D_n^-\right)\psi_{D,n}\left(x_p, y_p\right) + \frac{T_{22}^m}{\rho_0 \omega}\sum_{n=1}^{N_m} k_{D,n}\left(D_n^+ - D_n^-\right)\psi_{D,n}\left(x_p, y_p\right).\end{aligned} \quad (16)$$

It is worth noting here that equations (15) and (16) associated with the monolith imply all the wave amplitudes of chambers B and D, and thus a coupled system of equations is obtained. As will be seen later when applying the mode matching method, this situation can be improved from a computational point of view by using the orthogonality properties of the transversal modes [16, 25-29, 34].

2.2.3. Contraction

Finally, the contraction is considered. The condition of pressure continuity associated with Eq. (9) is written at N_e points over S_E given by coordinates (x_p, y_p, $z'' = L_D$) for chamber D

and (x_p, y_p, $z''' = 0$) for duct E. The corresponding set of equations can be expressed, for $p = 1, 2, \ldots, N_e$, as

$$\sum_{n=1}^{N_m}\left(D_n^+ \mathrm{e}^{-\mathrm{j}k_{D,n}L_D} + D_n^- \mathrm{e}^{\mathrm{j}k_{D,n}L_D}\right)\psi_{D,n}\left(x_p, y_p\right) = \sum_{n=1}^{N_e}\left(E_n^+ + E_n^-\right)\psi_{E,n}\left(x_p, y_p\right). \quad (17)$$

At the same points over S_E, the continuity of axial acoustic velocity (10) yields

$$\sum_{n=1}^{N_m} k_{D,n}\left(D_n^+ \mathrm{e}^{-\mathrm{j}k_{D,n}L_D} - D_n^- \mathrm{e}^{\mathrm{j}k_{D,n}L_D}\right)\psi_{D,n}\left(x_p, y_p\right) = \sum_{n=1}^{N_e} k_{E,n}\left(E_n^+ - E_n^-\right)\psi_{E,n}\left(x_p, y_p\right). \quad (18)$$

For the right end rigid plate characterized by Eq. (11), $N_m - N_e$ points with coordinates (x_p, y_p, $z'' = L_D$) are chosen over $S_D - S_E$. The associated set of equations is, for $p = 1, 2, \ldots, N_m - N_e$,

$$\sum_{n=1}^{N_m} k_{D,n}\left(D_n^+ \mathrm{e}^{-\mathrm{j}k_{D,n}L_D} - D_n^- \mathrm{e}^{\mathrm{j}k_{D,n}L_D}\right)\psi_{D,n}\left(x_p, y_p\right) = 0. \quad (19)$$

The explicit form of Eqs. (12)-(19) for the particular case of configurations with circular cross-section will be provided in section 2.4.

2.3. Mode-matching method

A weighted integration procedure is used here for Eqs. (3)-(11), whose weighting functions are the transversal modes of the ducts [5, 6, 25-29, 33]. To apply the mode matching method, a number of modes N_m is considered again to expand the acoustic pressure and velocity fields, Eqs. (1) and (2), for regions B and D, associated with the chambers, while N_a and N_e modes are taken into account for the inlet and outlet ducts A and E, respectively. To compute the unknown wave amplitudes, an algebraic system of equations is generated as follows.

2.3.1. Expansion

Starting with the expansion, multiply first Eq. (3) (continuity of pressure) by the transversal mode $\psi_{A,s}\left(x, y\right)$, with $s = 1, 2, \ldots, N_a$, and integrate over S_A. This yields

$$\int_{S_A} P_A\left(x, y, z=0\right)\psi_{A,s}\left(x, y\right)dS = \int_{S_A} P_B\left(x, y, z'=-L_B\right)\psi_{A,s}\left(x, y\right)dS. \quad (20)$$

The orthogonality properties of the transversal modes [25-29, 33, 34] lead, for $s = 1, 2, \ldots, N_a$, to

$$\left(A_s^+ + A_s^-\right)\int_{S_A} \psi_{A,s}^2\left(x,y\right)dS$$
$$= \sum_{n=1}^{N_m}\left(B_n^+ \, \mathrm{e}^{-\mathrm{j}k_{B,n}\left(-L_B\right)} + B_n^- \, \mathrm{e}^{\mathrm{j}k_{B,n}\left(-L_B\right)}\right)\int_{S_A} \psi_{B,n}\left(x,y\right)\psi_{A,s}\left(x,y\right)dS. \tag{21}$$

Eqs. (4) and (5), related to the axial velocity at the expansion, are multiplied by the transversal mode $\psi_{B,s}\left(x,y\right)$, with s = 1, 2, ..., N_m. The former product is integrated over S_A and the latter over $S_B - S_A$, leading after summation to

$$\int_{S_A} U_A\left(x,y,z=0\right)\psi_{B,s}\left(x,y\right)dS = \int_{S_B} U_B\left(x,y,z'=-L_B\right)\psi_{B,s}\left(x,y\right)dS. \tag{22}$$

As indicated previously, for s = 1, 2, ..., N_m, the orthogonality properties of the transversal modes yield

$$\sum_{n=1}^{N_a} k_{A,n}\left(A_n^+ - A_n^-\right)\int_{S_A} \psi_{A,n}\left(x,y\right)\psi_{B,s}\left(x,y\right)dS$$
$$= k_{B,s}\left(B_s^+ \, \mathrm{e}^{-\mathrm{j}k_{B,s}\left(-L_B\right)} - B_s^- \, \mathrm{e}^{\mathrm{j}k_{B,s}\left(-L_B\right)}\right)\int_{S_B} \psi_{B,s}^2\left(x,y\right)dS. \tag{23}$$

2.3.2. Monolith

The same approach is applied to Eqs. (6)-(8), associated with the four-pole relation between the acoustic pressure and axial velocity at both sides of the monolith. These equations are multiplied by the transversal mode $\psi_{B,s}\left(x,y\right) = \psi_{D,s}\left(x,y\right)$, with s = 1, 2, ..., N_m. Integrating over $S_B \equiv S_D$, taking advantage of the orthogonality relations and removing common factors, the following equations are derived for s = 1, 2, ..., N_m

$$B_s^+ + B_s^- = T_{11}^m\left(D_s^+ + D_s^-\right) + T_{12}^m \frac{k_{D,s}}{\rho_0 \, \omega}\left(D_s^+ - D_s^-\right), \tag{24}$$

$$\frac{k_{B,s}}{\rho_0 \, \omega}\left(B_s^+ - B_s^-\right) = T_{21}^m\left(D_s^+ + D_s^-\right) + T_{22}^m \frac{k_{D,s}}{\rho_0 \, \omega}\left(D_s^+ - D_s^-\right). \tag{25}$$

Compared to Eqs. (15) and (16), associated with the point collocation technique, it is interesting to note that very simple algebraic expressions (24) and (25) have been obtained with the mode matching method, where neither integrations nor modal summations appear. In addition, Eqs. (24) and (25) do not depend on the geometry of the transversal cross-section (provided that this is axially uniform) and relate directly wave amplitudes with equal modal number [6, 28]. As shown later, the computational performance of this approach will deliver better results when compared to alternative methods such as the point collocation technique. A clear advantage is also obtained when

applying the mode matching method to cylindrical ducts over other geometries involving non-uniform cross-section, such as conical pipes [5].

2.3.3. Contraction

Finally, similar to the approach presented for the expansion, Eqs. (9)-(11) associated with the contraction provide a final set of equations as follows. The pressure condition (9) is multiplied by the transversal mode $\psi_{E,s}(x,y)$, with s = 1, 2, ..., N_e, and integrated over S_E, leading to

$$\sum_{n=1}^{N_m}\left(D_n^+ \mathrm{e}^{-\mathrm{j}k_{D,s}L_D} + D_n^- \mathrm{e}^{\mathrm{j}k_{D,s}L_D}\right)\int_{S_E}\psi_{D,n}(x,y)\psi_{E,s}(x,y)dS = \left(E_s^+ + E_s^-\right)\int_{S_E}\psi_{E,s}^2(x,y)dS, \tag{26}$$

where the orthogonality properties have already been taken into account. On the other hand, the velocity conditions (10) and (11) yield, after multiplication by $\psi_{D,s}(x,y)$, integration and summation, the following expression

$$k_{D,s}\left(D_s^+ \mathrm{e}^{-\mathrm{j}k_{D,s}L_D} - D_s^- \mathrm{e}^{\mathrm{j}k_{D,s}L_D}\right)\int_{S_D}\psi_{D,s}^2(x,y)dS = \sum_{n=1}^{N_e}k_{E,n}\left(E_n^+ - E_n^-\right)\int_{S_E}\psi_{E,n}(x,y)\psi_{D,s}(x,y)dS, \tag{27}$$

with s = 1, 2, ..., N_m, and where, again, orthogonality has been considered.

Analytical expressions for the integrals of Eqs. (20)-(27) are provided in section 2.4 for the particular case of geometries with circular cross-section.

2.4. Configurations with circular cross-section

For illustration purposes, concentric geometries having circular cross-section are considered hereafter. Thus, only axisymmetric terms are retained in the modal expansions of the ducts and chambers involved. The transversal (radial) mode for region A can be written as [16, 25-28]

$$\psi_{A,n} = \psi_{A,n}(r) = \mathrm{J}_0(\alpha_n r/R_1), \tag{28}$$

R_1 being the duct radius, J_0 the zeroth-order Bessel function of the first kind, and α_n the n-th root satisfying the rigid wall boundary condition $\mathrm{J}_0'(\alpha_n)=0$ [16, 34]. Eq. (28) is also

valid for chambers *B* and *D*, with radius R_2, and duct *E* considering the corresponding radius R_3. The axial wavenumber is given by

$$k_{A,n} = \pm\sqrt{k_0^2 - \left(\alpha_n / R_1\right)^2}, \tag{29}$$

$k_0 = \omega / c_0$ being the wavenumber in air. The signs associated with the axial wavenumbers are chosen to guarantee exponential attenuation of evanescent modes [25-28].

Therefore, for the case of axisymmetric configurations, the transversal modes of the point collocation expressions detailed by Eqs. (12)-(19) are computed as follows

$$\psi_{A,n} = \mathrm{J}_0\left(\alpha_n r_p / R_1\right) \qquad \text{for } 0 \le r_p \le R_1, \tag{30}$$

$$\psi_{B,n} = \psi_{D,n} = \mathrm{J}_0\left(\alpha_n r_p / R_2\right) \qquad \text{for } 0 \le r_p \le R_2, \tag{31}$$

$$\psi_{E,n} = \mathrm{J}_0\left(\alpha_n r_p / R_3\right) \qquad \text{for } 0 \le r_p \le R_3. \tag{32}$$

Regarding the mode matching method, the integrals of Eqs. (20)-(23), (26) and (27) can be computed analytically, thus reducing the computational effort. The final system of equations for axisymmetric configurations is detailed next. In the case of the expansion, Eq. (21) is written as

$$\left(A_s^+ + A_s^-\right) R_1^2 \mathrm{J}_0^2\left(\alpha_s\right) = \sum_{n=1}^{N_m} \left(B_n^+ \mathrm{e}^{-\mathrm{j}k_{B,n}\left(-L_B\right)} + B_n^- \mathrm{e}^{\mathrm{j}k_{B,n}\left(-L_B\right)}\right) \mathfrak{R}_1, \tag{33}$$

while Eq. (23) now reads

$$\sum_{n=1}^{N_a} k_{A,n}\left(A_n^+ - A_n^-\right) \mathfrak{R}_2 = k_{B,s}\left(B_s^+ \mathrm{e}^{-\mathrm{j}k_{B,s}\left(-L_B\right)} - B_s^- \mathrm{e}^{\mathrm{j}k_{B,s}\left(-L_B\right)}\right) R_2^2 \mathrm{J}_0^2\left(\alpha_s\right). \tag{34}$$

In Eqs. (33) and (34), the corresponding integrals (including $\mathfrak{R}_1$ and $\mathfrak{R}_2$), have been computed through the expressions detailed in the Appendix A. For the coupling between the ducts *B* and *D* at both sides of the monolith, Eqs. (24) and (25) are used directly. As mentioned previously, no dependence exists on the particular chamber cross-section for the problem under consideration due the orthogonality of the transversal modes [6, 28]. These equations are repeated here for convenience,

$$B_s^+ + B_s^- = T_{11}^m\left(D_s^+ + D_s^-\right) + T_{12}^m \frac{k_{D,s}}{\rho_0 \omega}\left(D_s^+ - D_s^-\right), \tag{35}$$

$$\frac{k_{B,s}}{\rho_0\,\omega}\left(B_s^+ - B_s^-\right) = T_{21}^m\left(D_s^+ + D_s^-\right) + T_{22}^m\frac{k_{D,s}}{\rho_0\,\omega}\left(D_s^+ - D_s^-\right). \tag{36}$$

In the case of the contraction consisting of ducts *D* and *E*, Eq. (26) is now written as

$$\sum_{n=1}^{N_m}\left(D_n^+\,\mathrm{e}^{-\mathrm{j}k_{D,s}L_D} + D_n^-\,\mathrm{e}^{\mathrm{j}k_{D,s}L_D}\right)\Re_3 = \left(E_s^+ + E_s^-\right)R_3^2\,\mathrm{J}_0^2\left(\alpha_s\right), \tag{37}$$

and Eq. (27) can be finally expressed by

$$k_{D,s}\left(D_s^+\,\mathrm{e}^{-\mathrm{j}k_{D,s}L_D} - D_s^-\,\mathrm{e}^{\mathrm{j}k_{D,s}L_D}\right)R_2^2\,\mathrm{J}_0^2\left(\alpha_s\right) = \sum_{n=1}^{N_e}k_{E,n}\left(E_n^+ - E_n^-\right)\Re_4. \tag{38}$$

The computation of the integrals (including $\Re_3$ and $\Re_4$) in Eqs. (37) and (38) has been carried out through the expressions detailed in the Appendix A.

To determine the acoustic attenuation of the exhaust device, the transmission loss (*TL*) can be evaluated [16]. First, the modal amplitudes $A_n^{\pm}$, $B_n^{\pm}$, $D_n^{\pm}$ and $E_n^{\pm}$ are computed. Eqs. (12)-(19) define the algebraic system to be solved if the point collocation technique is used, consisting of $N_a + 4\,N_m + N_e$ equations. On the other hand, Eqs. (33)-(38) provide the algebraic system corresponding to the mode matching method, having also $N_a + 4\,N_m + N_e$ equations. In both cases, the additional equations for *TL* computation [16] can be $A_0^+ = 1$, $A_n^+ = 0$, $\forall n$ (incident plane wave) and $E_n^- = 0 \;\; \forall n$ (anechoic termination). Once the modal amplitudes are solved, *TL* is given by

$$TL = -20\log\left(\frac{R_3}{R_1}\left|E_0^+\right|\right). \tag{39}$$

For the dimensions and frequency range considered in the current investigation, the higher order modes leaving the chamber *D* in the outlet duct *E* will decay rapidly with distance, and therefore *TL* is uniquely defined with independence of location [28].

3. RESULTS AND DISCUSSION

To obtain results with the proposed models, a specific catalytic converter configuration is considered. The ducts and chambers are defined by the dimensions $R_1 = R_3 = 0.0268$ m (radii of the inlet and outlet ducts A and E, respectively), $R_2 = 0.15$ m (radius of the chambers B and D at both sides of the monolith) and $L_B = L_D = 0.1$ m (see Fig. 1 for details). Cold flow hypotheses are assumed in the calculations [33], the properties of the air being $c_0 = 340$ m/s and $\rho_0 = 1.225$ kg/m^3 (speed of sound and density, respectively). Concerning the acoustic model of the monolith, it is characterized by the following values: length $L_C = 0.2$ m, resistivity $R = 1000$ rayl/m, $\phi = 0.8$, geometric factor $\alpha_g = 1.07$, dynamic viscosity $\mu = 1.783 \cdot 10^{-5}$ Pa s, thermal conductivity $\kappa = 0.02534$ W/(m K) and specific heat at constant pressure $C_p = 1005$ J/(kg K). The detailed model for the four-pole matrix computation can be found in the literature [2, 6, 8, 18, 34].

3.1. Validation

First, the proposed analytical techniques based on point collocation and mode matching are validated by comparison with a reference numerical solution computed through FEM [8, 16]. The numerical calculations have been carried out with a refined finite element mesh consisting of axisymmetric 8-node quadratic quadrilateral elements, whose approximate size is 0.0015 m. This provides 70 quadratic elements per wavelength for the maximum frequency $f_{max} = 3200$ Hz considered in the simulations, thus guaranteeing an accurate reference. For the point collocation technique, four solutions have been obtained with: (1) $N_m = 4$ points in the chambers and $N_a = N_e = 1$ point in the inlet/outlet ducts; (2) $N_m = 10$ and $N_a = N_e = 2$; (3) $N_m = 40$ and $N_a = N_e = 8$; and finally (4) $N_m = 75$ and $N_a = N_e = 14$. Regarding the mode matching method, three solutions are considered, with the following number of modes: (1) $N_m = 2$ and $N_a = N_e = 1$; (2) $N_m = 4$ and $N_a = N_e = 1$; and (3) $N_m = 10$ and $N_a = N_e = 2$. More information about the influence of N_m on the results will be provided in section 3.2. Figs. 2 and 3 show the analytical results of the point collocation technique (PC) and the mode matching method (MM), respectively, as well as the reference FEM solution. As it can be seen, a suitable convergence appears as the number of collocation points/modes increases. The agreement for the highest numbers is excellent, with undistinguishable curves over all the frequency range, thus validating the proposed analytical techniques from a practical point of view. In addition, it is worth noting that, with the dimensions previously defined for ducts B and D, as well as the speed of sound c_0 considered in the computations, the first radial mode starts propagating at 1382 Hz [16]. A steep reduction of the catalytic converter noise attenuation performance is observed in Figs. 2 and 3 above this frequency, which would not have been predicted if only plane

waves had been modelled in all the ducts involved. Thus, the multidimensional approach adopted here overcomes the limitations of a pure plane wave model [16] and avoids potential transmission loss overestimation

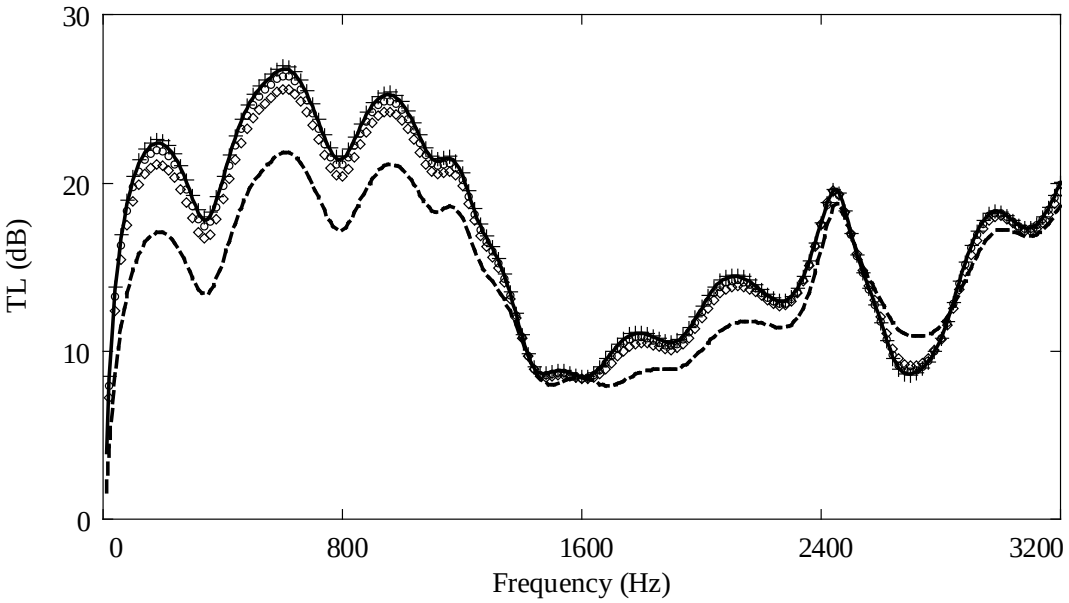

Fig. 2. *TL* of a catalytic converter with monolith: + + +, FEM; – – –, PC, N_m = 4; ◊ ◊ ◊, PC, N_m = 10; o o o, PC, N_m = 40; —, PC, N_m = 75.

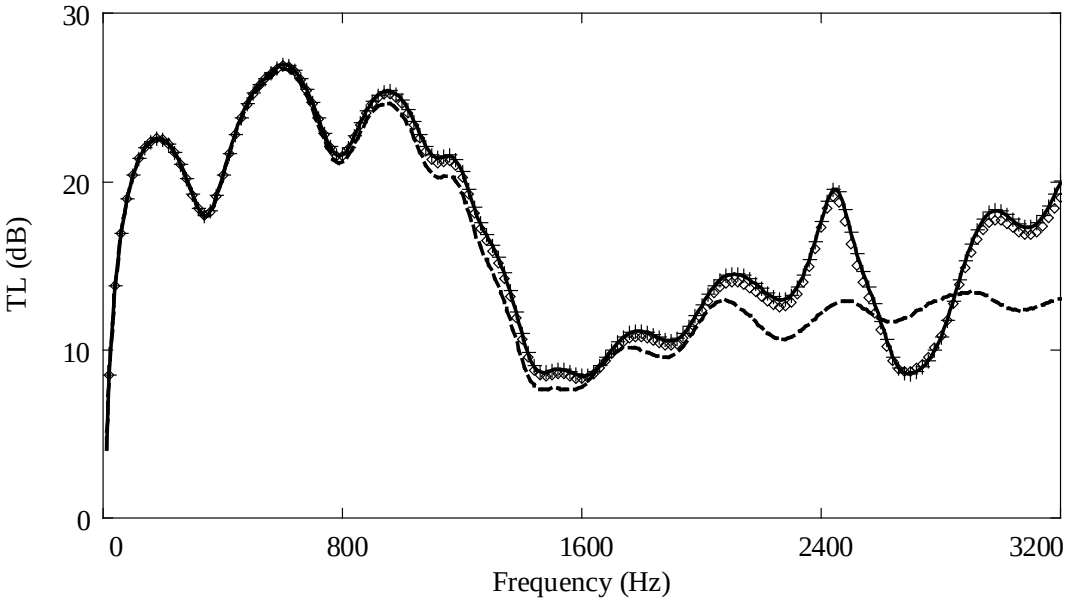

Fig. 3. *TL* of a catalytic converter with monolith: + + +, FEM; – – –, MM, N_m = 2; ◊ ◊ ◊, MM, N_m = 4; —, MM, N_m = 10.

3.2. Comparison of approaches

The proposed analytical techniques are compared in this section in terms of their computational performance. From the previous results (see Figs. 2 and 3), it is inferred that the solution converges as the number of collocation points/modes increases. This aspect is further confirmed by the results presented in Fig. 4, where the *TL* relative error [8, 24] is reduced for higher N_m. The error has been computed with the reference numerical solution obtained through FEM in section 3.1. For the mode matching method, the decreasing error exhibits a more uniform trend (note that log-log scale is used), while the point collocation technique presents a less uniform behaviour.

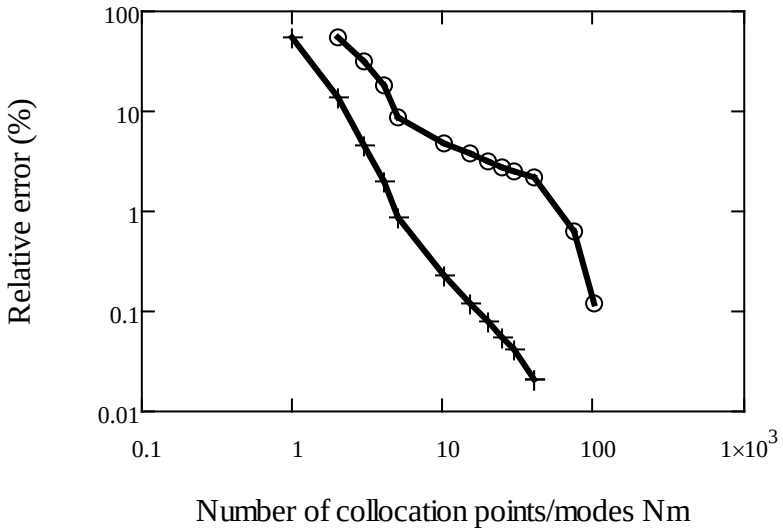

Fig. 4. Computational performance of the proposed tools. Relative error (%) versus number of collocation points/modes: —o—, point collocation; —+—, mode matching.

The computation time is depicted in Fig. 5 and increases for higher N_m, as expected. Anyway, it is worth mentioning that, based on a number of numerical experiments, the computational effort in the case of the two proposed techniques improves the time expenditure of FEM, mainly when mode matching is used. For a commercial general purpose FE program, the preprocessing tasks (including mesh generation), solution and postprocessing could easily take more than an hour. A considerable reduction in the computational cost can be achieved by implementing a specific in-house FE code for the particular problem under investigation, where the aforementioned tasks are automated. In this latter case, computation times depend mainly on the approximate desired error, for which the most important features are the element size and the interpolation degree [8].

For values of error being acceptable from a practical point of view (for example, lower than 5%), computation times are detailed next. For two-dimensional axisymmetric problems modelled with 8-node quadratic quadrilateral elements, times can be of the order of tens of seconds, while at least several tens of minutes can be required for three-dimensional problems with 20-node quadratic hexahedral elements. These approximate times are associated with FE results computed on an Intel Core i7, 3.4 GHz machine with 8 GB of RAM.

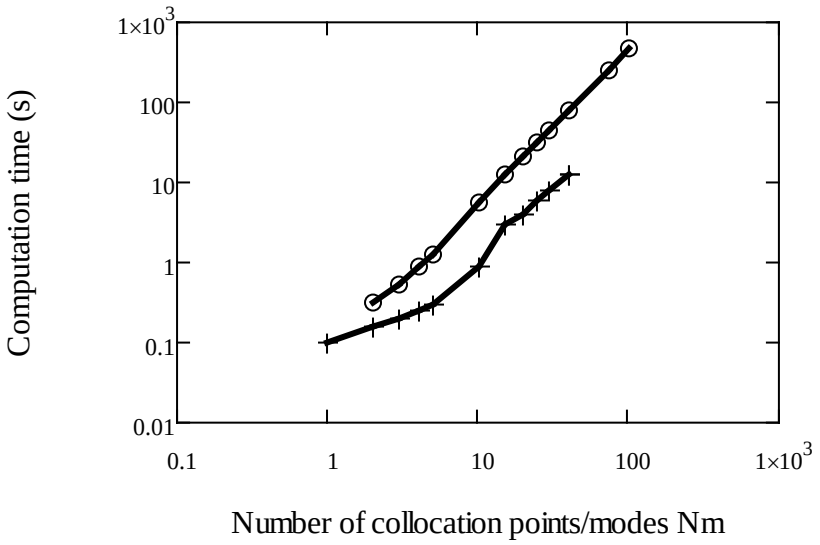

Fig. 5. Computational performance of the proposed tools. Computation time (s) versus number of collocation points/modes: —o—, point collocation; —+—, mode matching.

Finally, the curves shown in Fig. 6 provide a powerful illustration that, for a given relative error, the mode matching technique delivers a lower computation time. Therefore, mode matching should be the preferred simulation tool, at least for the specific problem under consideration. One of the main reasons seems to be related to the orthogonality properties of the transversal modes for ducts with axially uniform cross-section. For ducts with variable transversal geometry (e.g. conical), where an analytical description of the wave propagation can be given in terms of spherical Hankel and Legendre functions, it is expected that the differences are not so favourable to mode matching [5, 9]. The same can be said in those cases in which there are no analytical formulas of the type shown in Appendix A to evaluate the integrals over the transversal area. A potential possibility in the case of geometries of arbitrary but axially uniform cross-section could be the use of a hybrid approach combining point collocation at the expansions and contractions together with mode matching Eqs. (35) and (36) for the monolith.

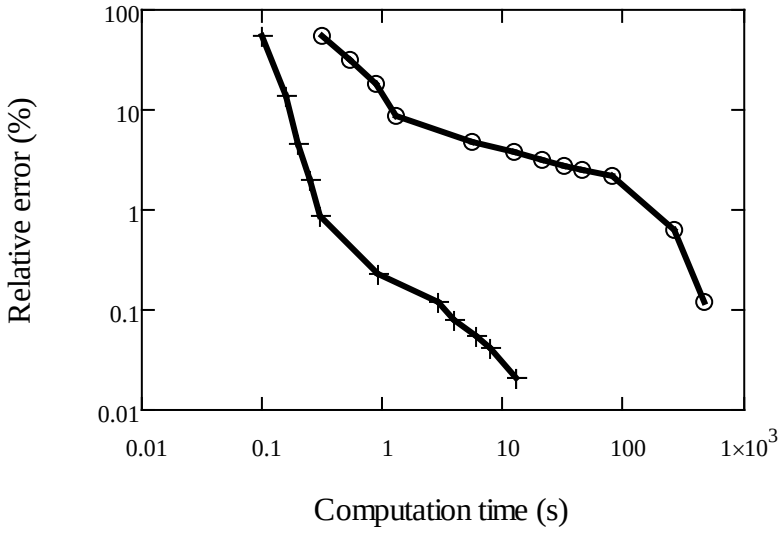

Fig. 6. Computational performance of the proposed tools. Relative error (%) versus computation time (s): —o—, point collocation; —+—, mode matching.

3.3. Influence of location for collocation points

Finally, Fig. 7 shows the impact of several collocation schemes on the *TL* assessment. In particular, a number of possibilities are considered whose difference lies in the treatment given to the points located at the vertices of expansion and contraction, with coordinates (r_p = R_1, z = 0) and (r_p = R_3, z''' = 0). In these vertices, a theoretical singularity of the acoustic field occurs, since axial velocity continuity conditions given by Eqs. (13) and (18) and zero axial velocity defined by Eqs. (14) and (19) can be applied simultaneously. The results depicted in Fig. 7 correspond to four location possibilities, all of them computed with N_m = 25 for comparison purposes. Option 1 includes the singular points in Eqs. (12), (13), (17) and (18), but not in Eqs. (14) and (19). Option 2 uses the singular points in Eqs. (14) and (19) but not in (12), (13), (17) and (18). On the other hand, option 3 considers the singular point in all the previous equations and, finally, option 4 completely excludes the vertices of the collocation procedure. From the attenuation curves shown in Fig. 7, it is clear that the collocation scheme has a considerable influence on the results. Option 4, corresponding to the exclusion of vertices in all the equations, gives better results than the rest of approaches. On the contrary option 3, which uses these points in the area changes equations, seems to deliver the worst *TL* predictions. In fact, negative attenuations have even been obtained for certain N_m values with this option, which has no physical sense. Therefore, it can be deduced from the computations shown in Fig. 7 that it is convenient to

exclude the vertices of the geometrical discontinuities from the point collocation technique.

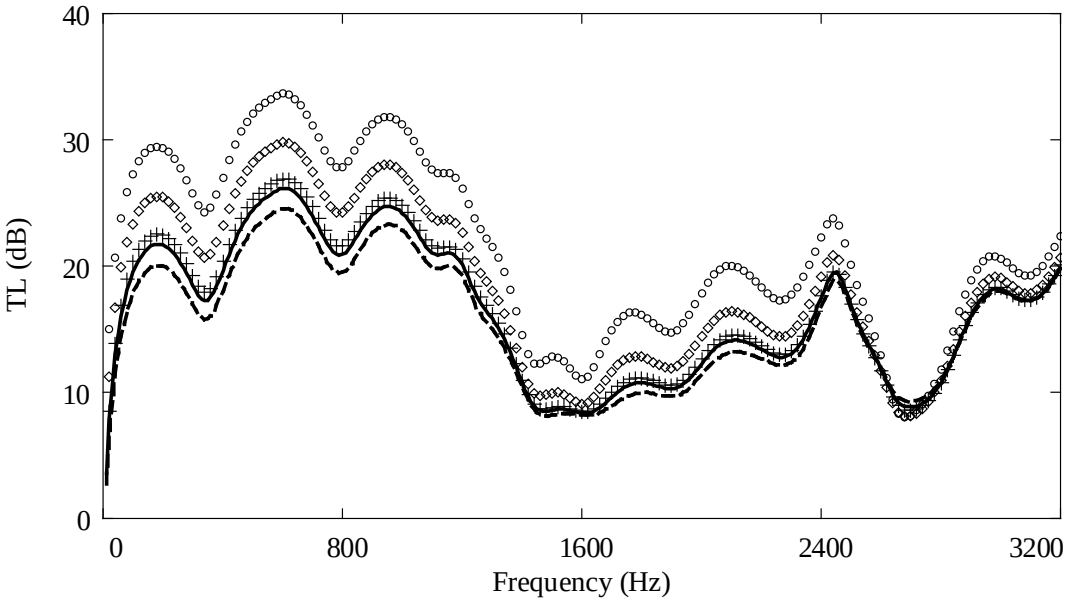

Fig. 7. *TL* of a catalytic converter with monolith: + + +, FEM; – – –, PC, option 1; ◊ ◊ ◊, PC, option 2; o o o, PC, option 3; —, PC, option 4.

4. CONCLUSIONS

Two analytical models based on the point collocation technique and the mode matching method have been presented in this work to assess the acoustic behaviour of automotive exhaust devices incorporating monoliths. The modelling methodology includes higher order modes in the ducts and chambers to guarantee accurate predictions in the high frequency range, while the monolith has been replaced by an acoustic four-pole transfer matrix to provide more realistic results. After validation by benchmarking against the FEM, both analytical techniques have been compared in terms of accuracy and speed. The approaches proposed in this work have been shown to provide accurate predictions of the device attenuation performance and to outperform the computational expenditure of a FEM computation. Some differences are found, however, between point collocation and mode matching in terms of computational speed and solution accuracy. From the results presented here, the most efficient technique for the particular configurations under study is the mode matching method since, for a given error, it is shown to be significantly faster than point collocation. The reasons may be attributed, among others, to orthogonality properties of the transversal modes. In addition, the location of the points has been shown

to have a significant influence on the results of the point collocation technique. In this sense, it has been concluded from the simulations that it is convenient to avoid the singular points located at the vertices of the area changes.

ACKNOWLEDGEMENTS

This work has been supported by Ministerio de Economía y Competitividad and the European Regional Development Fund (project TRA2013-45596-C2-1-R), as well as Generalitat Valenciana (projects Prometeo/2016/007 and GV/2016/011 of Conselleria d'Educació, Investigació, Cultura i Esport).

REFERENCES

[1] H. Zhao (editor), Advanced Direct Injection Combustion Technologies and Development, CRC Press, 2010. ISBN 978-1-4398-2475-7.

[2] A. Selamet, V. Easwaran, J. M. Novak, R. A. Kach. Wave attenuation in catalytic converters: reactive versus dissipative effects, Journal of the Acoustical Society of America, 103 (1998), 935–943.

[3] N. S. Dickey, A. Selamet, K. D. Miazgowicz, K. V. Tallio, S. J. Parks. Time domain computational modeling of viscothermal acoustic propagation in catalytic converter substrates with porous walls, Journal of the Acoustical Society of America, 118 (2005), 806-817.

[4] S. Allam, M. Åbom. Sound propagation in an array of narrow porous channels with application to diesel particulate filters, Journal of Sound and Vibration, 291 (2006), 882-901.

[5] F. D. Denia, L. Baeza, R. Kirby, A. Selamet. A multidimensional analytical study of sound attenuation in catalytic converters, 39th International Congress and Exposition on Noise Control Engineering (Inter-noise), Lisbon, Portugal, (2010).

[6] A. G. Antebas. Contribution to the acoustic modelling of the exhaust system in internal combustion engines. Application to silencers and catalytic converters (in Spanish), Doctoral Thesis, Universitat Politècnica de València, Valencia, (2010).

[7] C. Jiang, T. W. Wu, M. B. Xu, C. Y. R. Cheng. BEM modeling of mufflers with diesel particulate filters and catalytic converters, Noise Control Engineering Journal, 58 (2010), 243-250.

[8] F. D. Denia, J. Martínez-Casas, L. Baeza, F. J. Fuenmayor. Acoustic modelling of exhaust devices with nonconforming finite element meshes and transfer matrices, Applied Acoustics, 73 (2012), 713-722.

[9] F. D. Denia, E. M. Sánchez-Orgaz, J. Carballeira, F. J. Fuenmayor. Point collocation model for the acoustic behaviour of conical catalytic converters (in Spanish), Tecniacústica 2015, 46th Spanish Congress on Acoustics, Valencia, Spain, (2015).

[10] G. Kirchhoff. Ueber den einfluss der wärmeleitung in einem gase auf die schallbewegung, Annalen der Physik und Chemie, 134 (1868), 177-193.

[11] C. Zwikker, C. W. Kosten. Sound Absorbing Materials, Elsevier, 1949.

[12] M. R. Stinson. The propagation of plane sound waves in narrow and wide circular tubes, and generalization to uniform tubes of arbitrary cross-sectional shape, Journal of the Acoustical Society of America, 89 (1991), 550-558.

[13] H. S. Roh, W. P. Arnott, J. M. Sabatier, R. Raspet. Measurement and calculation of acoustic propagation constants in arrays of small air-filled rectangular tubes, Journal of the Acoustical Society of America, 89 (1991), 2617-2624.

[14] E. Dokumaci. Sound transmission in narrow pipes with superimposed uniform mean flow and acoustic modelling of automobile catalytic converters, Journal of Sound and Vibration, 182 (1995), 799-808.

[15] E. Dokumaci. On transmission of sound in circular and rectangular narrow pipes with superimposed mean flow, Journal of Sound and Vibration, 210 (1998), 375-389.

[16] M. L. Munjal. Acoustics of Ducts and Mufflers, Wiley, 2014. ISBN: 978-1-118-44312-5.

[17] F. D. Denia, A. G. Antebas, R. Kirby, F. J. Fuenmayor. Multidimensional acoustic modelling of catalytic converters, 16th International Congress on Sound and Vibration, Kraków, Poland (2009).

[18] J. F. Allard, N. Atalla. Propagation of Sound in Porous Media, Wiley, 2009. ISBN: 978-0-470-746615-0.

[19] R. Glav. The point-matching method on dissipative silencers of arbitrary cross-section, Journal of Sound and Vibration, 189 (1996), 123-135.

[20] R. Glav. The transfer matrix for a dissipative silencer of arbitrary cross-section, Journal of Sound and Vibration, 236 (2000), 575-594.

[21] R. Kirby, J. B. Lawrie. A point collocation approach to modelling large dissipative silencers, Journal of Sound and Vibration, 286 (2005), 313-339.

[22] R. Kirby. Transmission loss predictions for dissipative silencers of arbitrary cross section in the presence of mean flow, Journal of the Acoustical Society of America, 114 (2003), 200-209.

[23] L. Yang, Z. L. Ji, T. W. Wu. Transmission loss prediction of silencers by using combined boundary element method and point collocation approach, Engineering Analysis with Boundary Elements, 61 (2015), 265-273.

[24] F. D. Denia, E. M. Sánchez-Orgaz, L. Baeza, R. Kirby. Point collocation scheme in silencers with temperature gradient and mean flow, Journal of Computational and Applied Mathematics, 291 (2016), 127-141.

[25] R. Kirby, F. D. Denia. Analytic mode matching for a circular dissipative silencer containing mean flow and a perforated pipe, Journal of the Acoustical Society of America, 122 (2007), 3471-3482.

[26] F. D. Denia, A. Selamet, F. J. Fuenmayor, R. Kirby. Acoustic attenuation performance of perforated dissipative mufflers with empty inlet/outlet extensions, Journal of Sound and Vibration, 302 (2007), 1000-1017.

[27] R. Kirby. A comparison between analytic and numerical methods for modelling automotive dissipative silencers with mean flow, Journal of Sound and Vibration, 325 (2009), 565–582.

[28] F. D. Denia, A. G. Antebas, A. Selamet, A. M. Pedrosa. Acoustic characteristics of circular dissipative reversing chamber mufflers, Noise Control Engineering Journal, 59 (2011), 234-246.

[29] Z. Fang, Z. L. Ji. Numerical mode matching approach for acoustic attenuation predictions of double-chamber perforated tube dissipative silencers with mean flow, Journal of Computational Acoustics, 22 (2014), article number 1450004.

[30] Z. Fang, Z. L. Ji, C. Y. Liu. Acoustic attenuation analysis of silencers with multi-chamber by using coupling method based on subdomain division technique, Applied Acoustics, 116 (2017), 152–163.

[31] A. G. Antebas, F. D. Denia, A. M. Pedrosa, F. J. Fuenmayor. A finite element approach for the acoustic modeling of perforated dissipative mufflers with non-homogeneous properties, Mathematical and Computer Modelling, 57 (2013), 1970-1978.

[32] F. D. Denia, E. M. Sánchez-Orgaz, J. Martínez-Casas, R. Kirby. Finite element based acoustic analysis of dissipative silencers with high temperature and thermal-induced heterogeneity, Finite Elements in Analysis and Design, 101 (2015), 46-57.

[33] E. M. Sánchez-Orgaz. Advanced numerical techniques for the acoustic modelling of materials and noise control devices in the exhaust system of internal combustion engines, Doctoral Thesis, Universitat Politècnica de València, Valencia, (2016).

[34] F. P. Mechel. Formulas of Acoustics, Springer, 2008. ISBN: 978-3-540-76832-6.

[35] E. Rohan, V. Lukeš. Homogenization of the acoustic transmission through a perforated layer, Journal of Computational and Applied Mathematics, 234 (2010), 1876–1885.

[36] A. Mimani, M. L. Munjal. Acoustical behavior of single inlet and multiple outlet elliptical cylindrical chamber muffler, Noise Control Engineering Journal, 60 (2012), 605-626.

APPENDIX A

To carry out the analytical integration of transversal modes associated with the mode matching method, the following expression has been used [6, 16, 25, 26]

$$\int_0^R \mathrm{F}_0(\lambda r)\mathrm{G}_0(\mu r) r\,dr = \begin{cases} \dfrac{R}{\lambda^2-\mu^2}\left(\lambda \mathrm{F}_1(\lambda R)\mathrm{G}_0(\mu R) - \mu \mathrm{F}_0(\lambda R)\mathrm{G}_1(\mu R)\right), & \lambda \neq \mu, \\ \dfrac{R^2}{2}\left(\mathrm{F}_0(\lambda R)\mathrm{G}_0(\lambda R) + \mathrm{F}_1(\lambda R)\mathrm{G}_1(\lambda R)\right), & \lambda = \mu, \end{cases} \tag{A.1}$$

with F_0, G_0, F_1, and G_1 being the Bessel functions of any kind, and zeroth- and first-order, respectively.

Thus, the terms $\mathfrak{R}_1$, $\mathfrak{R}_2$, $\mathfrak{R}_3$, and $\mathfrak{R}_4$ of Eqs. (33), (34), (37) and (38)are given by

$$\mathfrak{R}_1 = \begin{cases} R_1^2 \mathrm{J}_0^2(\alpha_s), & \alpha_n/R_2 = \alpha_s/R_1, \\ \dfrac{\mathrm{J}_0(\alpha_s)\mathrm{J}_1(\alpha_n R_1/R_2) 2\alpha_n R_1/R_2}{(\alpha_n/R_2)^2 - (\alpha_s/R_1)^2}, & \alpha_n/R_2 \neq \alpha_s/R_1, \end{cases} \tag{A.2}$$

$$\Re_2=\begin{cases} R_1^2\,\mathrm{J}_0^2(\alpha_s), & \alpha_s/R_2=\alpha_n/R_1\,, \\ \dfrac{\mathrm{J}_0(\alpha_n)\mathrm{J}_1(\alpha_s R_1/R_2)2\alpha_s R_1/R_2}{(\alpha_s/R_2)^2-(\alpha_n/R_1)^2}, & \alpha_s/R_2\neq\alpha_n/R_1\,, \end{cases} \tag{A.3}$$

$$\Re_3=\begin{cases} R_3^2\,\mathrm{J}_0^2(\alpha_s), & \alpha_n/R_2=\alpha_s/R_3\,, \\ \dfrac{\mathrm{J}_0(\alpha_s)\mathrm{J}_1(\alpha_n R_3/R_2)2\alpha_n R_3/R_2}{(\alpha_n/R_2)^2-(\alpha_s/R_3)^2}, & \alpha_n/R_2\neq\alpha_s/R_3\,, \end{cases} \tag{A.4}$$

$$\Re_4=\begin{cases} R_3^2\,\mathrm{J}_0^2(\alpha_s), & \alpha_s/R_2=\alpha_n/R_3\,, \\ \dfrac{\mathrm{J}_0(\alpha_n)\mathrm{J}_1(\alpha_s R_3/R_2)2\alpha_s R_3/R_2}{(\alpha_s/R_2)^2-(\alpha_n/R_3)^2}, & \alpha_s/R_2\neq\alpha_n/R_3\,. \end{cases} \tag{A.5}$$